Mesoscopic FRET Antenna Materials by Self-Assembling Iridium(III) Complexes and BODIPY Dyes

Bagnall, Andrew J.; SantanaVega, Marina; Martinelli, Jonathan; Djanashvili, Kristina; Cucinotta, Fabio

Important note
To cite this publication, please use the final published version (if applicable).
Please check the document version above.

▌**Mesoporous Materials** │*Hot Paper*│

Mesoscopic FRET Antenna Materials by Self-Assembling Iridium(III) Complexes and BODIPY Dyes

Andrew J. Bagnall,[a] Marina Santana Vega,[a] Jonathan Martinelli,[b] Kristina Djanashvili,[b] and Fabio Cucinotta*[a]

Abstract: This study presents a new design of light-harvesting antenna materials using two dyes organised into mesoporous silica: an iridium(III) complex and a BODIPY-derived surfactant that undergo Förster resonance energy transfer (FRET), acting, respectively, as donor and acceptor. The chemical structure of each dye determines the position taken within the micellar templates used for the synthesis of the silica host, which maintains mesopore order as shown by TEM imaging. Steady-state and time-resolved UV-visible spectroscopy revealed that incorporation of the iridium complex into the silica shields it from oxygen-induced quenching and allows a degree of control over the donor–acceptor distance, yielding FRET efficiencies from 24 to 76% and tuneable emission ranges. Such silica-based antennae show promising properties for the realisation of polychromatic sensitisers for photovoltaics and photocatalysis.

Introduction

The development of optical materials for light-based technologies has witnessed a tremendous growth over the previous half-century, benefitting from advancements in the fields of photochemistry and supramolecular chemistry.[1–4] The latter one has provided a diverse wealth of accessible synthetic strategies to efficiently organise light-responsive components from the molecular level up to the material scale. Self-assembled systems made of organized multi-chromophoric units, mimicking the high levels of organisation featured by natural photosystems, have shown promise for application into photovoltaics and light-emitting technologies.[5–10]

The rise of nanotechnology has generated new opportunities and methods to target such applications, primarily through the design of materials with specific and tuneable photophysical and photochemical properties. In particular, nanoscale systems allow control over the organisation of chromophores into both space and energy dimensions, in such a way as to function as highly effective antennae able to capture light energy over the UV-visible range and modulate it through photo-in-

duced energy transfer cascade phenomena to achieve the desired luminescence output.[11]

A wide variety of such supramolecular photosystems have been constructed via self-assembly through non-covalent interactions and include dendrimers,[12–17] organogels,[18–20] multiporphyrin arrays,[21,22] biomaterials[23–26] carbon-based nanometric networks27 and quantum dots dispersed in polymeric films.[28] Furthermore, polymers have been used as effective means to promote the formation of self-organised structures such as nanoparticles,[29,30] nanofibres[31] and nanotubes,[32] where organic dyes are able to perform directional energy transfer, and intra- and inter-chain migration has also been demonstrated.[33]

One recent approach for designing energy conversion materials is to incorporate chromophores into channel-forming or porous inorganic and organic frameworks to produce supramolecular host-guest compounds (HGCs) which can act as arrays of optical antennae. Typical inorganic hosts are robust periodic nanostructured silica, alumina or aluminosilicate solids like zeolites.[34–36] Inclusion of dye molecules inside such frameworks is proven to result in homogeneous dispersion of the guest dyes, to enhance their optical stability, by making them less vulnerable to photo-degradation processes, owing to the ability to completely exclude oxygen and radical formation, and to confer mechanical and thermal robustness to the overall HGCs.[37–39] Importantly, the structure of a solid framework necessarily affects the photophysical properties of guest molecules in comparison to their solution or solid phase properties, restricting their vibrational and rotational freedom, controlling aggregation phenomena so as to suppress undesired emission quenching and induce an enhancement of luminescence, and also mediating interactions between guests such as energy transfer.[40–44]

Mesoporous silica frameworks, in particular, provide a good basis for the construction of HGCs with inbuilt optical function-

[a] A. J. Bagnall, M. Santana Vega, Dr. F. Cucinotta
School of Natural and Environmental Sciences, Newcastle University
Bedson Building, Queen Victoria Road, Newcastle upon Tyne, NE1 7RU (UK)
E-mail: fabio.cucinotta@newcastle.ac.uk

[b] Dr. J. Martinelli, Dr. K. Djanashvili
Department of Biotechnology, Delft University of Technology
Van der Maasweg 9, 2629 HZ Delft (The Netherlands)

⬚ Supporting information and the ORCID identification number(s) for the author(s) of this article can be found under:
https://doi.org/10.1002/chem.201802745.

alities. In mesoporous silica the large inner surface area per volume and the accessibility of their broad channel-like pores, controllable between 2 and 10 nm, make the frameworks well-suited to host a range of dye molecules and even catalysts.[45, 46] The typical synthesis of mesoporous silica is a two-steps route that utilises a micellar mesophase as a soft template around which the solid framework is constructed (Figure 1).
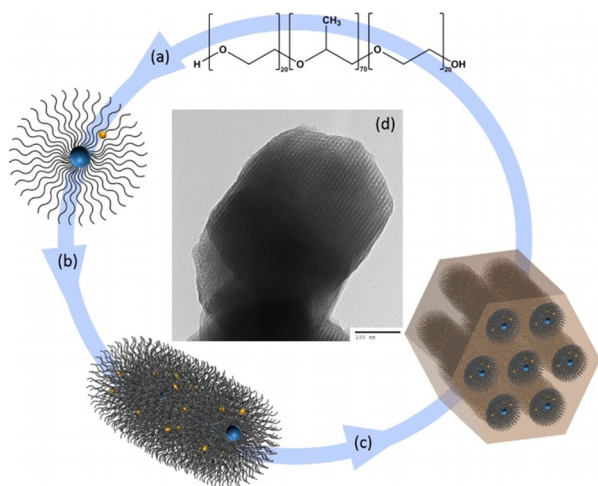

Figure 1. Diagram illustrating the preparation route of the dye-doped micellar template used for the construction of the mesoporous silica: (a) Formation of spherical micelles of P123, (b) transition to cylindrical micelles at the 2nd cmc, and (c) synthesis of the mesoporous silica host by polycondensation from monomeric silica precursor species. (d) TEM picture of a typical COK-12 particle. The blue and the yellow dots represent, respectively, the hydrophobic IrD complex and the JM dye with the hydrophilic PEG tail.

A relatively recent approach regarding the synthesis of photoactive HGCs is to position photoactive organic chromophores as part of the template and then allow the dyes to remain inside the mesopores.[47, 48] In such strategy, it is necessary to select an appropriate host framework which uses a template large enough so that can not be inordinately disrupted by the presence of the guest dye species and that can be synthesised under adequately mild conditions, avoiding the risk of chemical decomposition of the dye. A suitable host is the mesoporous silica named COK-12, whose synthesis utilises cylindrical micelles of the gemini surfactant Pluronic-P123 (see Figure 1), a triblock copolymer consisting of a hydrophobic polypropylene glycol (PPG) core (about 70 units) and a hydrophilic polyethylene glycol (PEG) tail (20 units) on either end of the chain, and quasi-neutral conditions (pH 6.5) to polymerise the silica precursor, sodium metasilicate, circumventing the need for strong acidic or basic conditions when using alkoxysilanes.[49]

Recently, we reported on the successful synthesis of analogous COK-12-based structures employing a BODIPY fluorophore embedded into Pluronic-P123 micelles.[47] Known for their excellent optical properties, namely large molar extinction

coefficients (over $10^5 \, M^{-1} \, cm^{-1}$), high fluorescence quantum yields and small Stokes shifts, BODIPYs have found a wide range of applications including as popular biological labelling reagents, chemosensors and laser dyes, and are promising candidates to be utilised as light-harvesting pigments in artificial photosynthetic systems, light-emitters in OLEDs, or as fluorescent switches.[50–55] When incorporated into mesoporous silica at low loadings of 1–5%, the green-emitting BODIPY derivative **JM** (see Figure 2) retains its exceptional properties, with fluorescence quantum yields up to 20%, and the hybrid material maintains its structural order, indicating a homogeneous dispersion of the dye into the structure. Nevertheless, such HGCs lack in poly-chromaticity, which is essential for the development of light-harvesting systems and white light emitters,[56] therefore a viable method of photosensitisation for the BODIPY chromophores in COK-12 must be pursued.
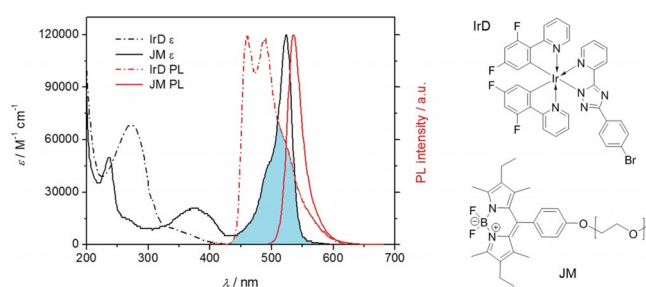
Figure 2. Structures of the IrD and JM dyes and their UV-visible absorption and emission profiles, with their spectral overlap as donor and acceptor, respectively.

In this study, we present a simple strategy to extend the photoactivity of mesoscopic materials across the visible spectrum, by incorporation, during the self-assembly process, of a second type of dye with contrasting absorption and emission regions to complement the first and engage in inter-species energy transfer processes, chiefly FRET. Moreover, in order to manipulate the efficiency of FRET and in turn the antenna-effects, we aim at controlling the distance between donor and acceptor units within the HGCs, acting on factors such as the localisation of dye species in the material and their concentration. For this purpose, we chose a cyclometalated, neutral iridium(III) complex with blue emission (**IrD** in Figure 2), which acts as energy donor for the BODIPY dye and positions itself within the hydrophobic core of the micellar template used for the construction of the HGCs (see Scheme in Figure 1).

Of particular advantage in this choice for a donor dye are (i) the relatively simple synthesis of cyclometalated iridium(III) complexes, (ii) the ease of tuneability of their emission colour through ligand design, (iii) their large molar extinction coefficients, up to $10^4 \, M^{-1} \, cm^{-1}$, (iv) high quantum yields of phosphorescence, up to 60%, owing to the large spin-orbit coupling constant of heavy metal centre ($\zeta_{Ir} = 3909 \, cm^{-1}$), and (v) their electroluminescence properties, which make them suitable for application in optoelectronic devices, such as light-emitting electrochemical cells (LEECs) and OLEDs.[57–65]

Furthermore, BODIPY dyes and metal complexes have been successfully used by Calzaferri and co-workers in the context of HGCs for trapping excitation energy from and injecting it into dye-loaded zeolite L materials, acting as stopcock molecules: in 2002, BODIPYs were the first stopcocks reported in the literature[54a] and two years later a ruthenium(II) compound was used as the first metal complex that demonstrated to inject excitation energy into an artificial antenna system.[54b] Following such pioneering studies, blue and green emitting iridium(III) complexes have also been subsequently used as energy injecting molecules to dye-loaded systems,[66] thus proving to have an exceptional potential to complement energy acceptor dyes such as BODIPYs.

Results and Discussion

Dye molecules

The cyclometalated heteroleptic iridium(III) complex, Ir(F$_2$ppy)$_2$(p-Br-ptap) (**IrD**), and the BODIPY compound N,N′-difluoroboryl-2,8-diethyl-1,3,7,9-tetramethyl-5-(4-ω-methoxy-PEG$_{2000}$-phenyl)-dipyrrin (**JM**) were synthesised according to previously reported procedures.[47,66] (see also the Experimental Section for further details). The UV-visible absorption and emission properties were also formerly elucidated and are recalled in Figure 2, with a particular focus on the spectral overlap between **IrD** emission and **JM** absorption, a key requisite for resonance energy transfer.

Briefly, **IrD** displays absorbance in the range 200–400 nm, with a molar extinction coefficient, ε, of $6.84 \times 10^4\,\text{M}^{-1}\,\text{cm}^{-1}$ at $\lambda_{\text{max}} = 272$ nm, and a ligand-centred phosphorescence emission with the first vibronic peak at 463 nm, quantum yield of 0.46 and excited state lifetime of 1.27 μs in deaerated solution (see also Table 1); **JM** shows a narrow absorption band, with a maximum peak around 522 nm and $\varepsilon = 1.1 \times 10^5\,\text{M}^{-1}\,\text{cm}^{-1}$, and an analogously sharp emission band centred at 534 nm, from the lowest excited singlet state, which has a lifetime of 6.05 ns and a fluorescence quantum yield of 0.44. The spectral overlap integral, hereafter J_{DA}, was calculated using a│e-UV/Vis-IR Spectral Software 2.2,[67] returning the value of 2.356×10^{15} nm^4 M^{-1} cm^{-1}.

Table 1. General photophysical data of the dyes in solution and in COK-12 HGCs.

Sample	Φ_{PL}[c]	τ_{PL} (%) [ns][d]	k_{R} [10^5 s^{-1}][e]	k_{NR} [10^5 s^{-1}][e]
IrD[a]	0.46	1274	3.61	4.24
1%IrD[b]	0.26	78 (27), 966 (17), 2705 (56)	0.96[f]	2.74[f]
5%IrD[b]	0.08	73 (50), 417 (23), 2356 (27)	0.34[f]	3.90[f]
1%IrD-1%JM[b]	–	79 (28), 655 (28), 2047 (44)	–	–
5%IrD-5%-JM[b]	–	72 (54), 288 (26), 568 (20)	–	–

[a] Deaerated 5.7×10^{-6} M acetonitrile solution. [b] Recorded from 0.3 mg mL^{-1} cyclohexane suspensions. [c] +/−0.01. [d] Recorded at $\lambda_{\text{em}} =$ 463 nm, using a 375 nm laser source (+/−50 ps). [e] (+/−8×10^3 s^{-1}). [f] Calculated from the longest lifetime component and Φ_{PL}.

Synthesis of the HGCs

The silica hybrid materials containing the two dyes were prepared using the modified templated synthesis depicted in Figure 1, where **JM**, having an average number of 45 -CH$_2$CH$_2$O- units, is embedded along the folded P123 chains, whereas the iridium(III) complex is expected to be localised inside the core hydrophobic region of the micelles, being totally insoluble in water. Donor–acceptor (D–A) 1:1 ratios were used in the construction of two HGCs which were prepared using D:A:P123 molar percentages of 1:1:98 and 5:5:90, yielding the samples named hereafter **1%IrD-1%JM** and **5%IrD-5%JM**, respectively. Overall dye loadings higher than 10% were avoided for two main reasons: i) to maintain the ordered hexagonal arrangement of the cylindrical micelles within the silica, which starts losing its long-scale order beyond the above dye loading,[47] and in turn to ensure the reliability of the geometrical model used to interpret the optical properties, and ii) to minimise the occurrence of potential triplet-triplet annihilation between **IrD** molecules, incurred by the closer proximity of dye molecules as their concentration increases, which would be detrimental for the efficiency of energy transfer between **IrD** and **JM** dyes. A low concentration of these molecules naturally leads to a greater average distance between them and reduces aggregation overall, making the assumption of a statistical distribution of intermolecular distances arising from a random spatial dispersion of dyes, which has indeed been applied in the literature to rationalise dye species behaviour in polymeric matrices;[55] additionally, the complexity of the excited state deactivation dynamics is expected to generally decrease with a reduction in aggregation processes, as fewer new radiative de-excitation pathways should arise.

Reference samples were also prepared for each of the two donor–acceptor systems, containing the donor species only (**1%IrD** and **5%IrD**) and the acceptor only (**1%JM** and **5%JM**), the latter two having been previously characterised.[47] All syntheses were carried out using a citrate buffer at pH 6.5, which does not alter the stability of the dyes, and the formation of mesoporous silica was achieved upon addition of a sodium silicate solution to the respective micellar phases (see Experimental for details). The resulting powdery insoluble materials were extracted and purified each time using vacuum filtration, aqueous washing and desiccation at ambient temperature. The washings of each sample were retained and analysed by absorption spectroscopy, to calculate the quantity of unincorporated dye via the Beer–Lambert law using the known molar extinction coefficient (see also Figure S1). In all cases, the extricated dye represented a negligible fraction of the starting reagent: the highest recorded percentage of unincorporated dye was 0.05%, from the synthesis of **1%IrD**.

The new hybrid materials were then characterized structurally and spectroscopically, in comparison with a standard sample of COK-12. The optical properties of the HGCs are hereafter described starting from the samples containing the donor species only and then comparing them to the corresponding D–A systems.

IrD in COK-12

The spectroscopic properties of the novel **IrD**-containing COK-12 HGCs were investigated by steady-state and time-resolved UV-visible emission spectroscopy, from 0.3 mg mL^{-1} suspensions. Cyclohexane was previously found to be an optimal medium for this purpose,[47] as the silica particles suspended within it can be finely dispersed to reduce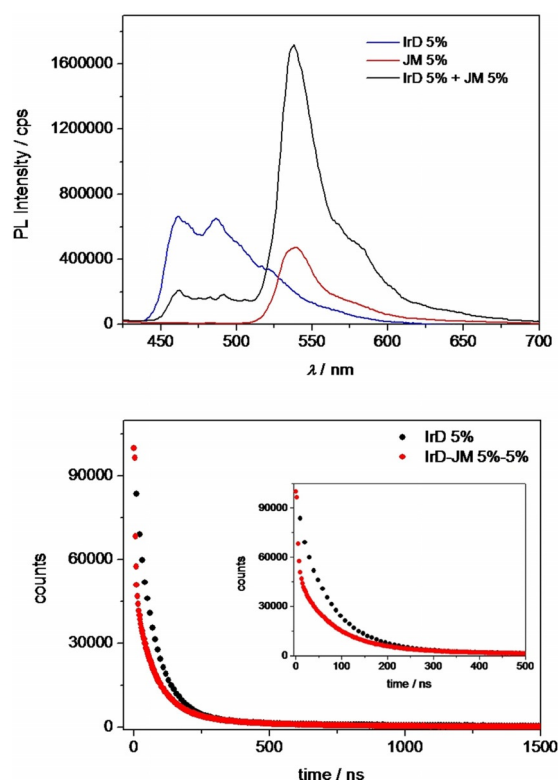 scattering and also due to its total ineffectiveness as solvents for both dyes, which ensures no leaching from the pores of the HGC.

The emission spectra of the complex in silica at different loadings (Figure 3 and Figure 4) show no changes in the profiles of the bands at 460 and 490 nm, as compared with the dye emission in acetonitrile solution, indicating that inclusion of **IrD** in the mesoporous silica has preserved its photochemical stability. Moreover, the time-resolved analysis shows some interesting effects that incorporation into the solid matrix has induced to the excited state of the complex.

The emission decay profiles (Figure 3 and Figure 4) were obtained using the time-correlated single-photon counting (TCSPC) technique and the fitted kinetic traces are reported in Table 1, which summarises the photophysical properties including the quantum yields. The kinetic profiles show multi-exponential excited state decays for both **1%IrD** and **5%IrD**, reflecting the presence of multiple deactivation pathways. Because of the complexity of the systems studied, we attribute

Figure 4. Top: Emission spectra of **5%IrD**, **5%JM** and **5%IrD-5%JM**, recorded from 0.3 mg mL^{-1} cyclohexane suspensions, at $\lambda_{exc}=300$ nm and 5 nm bandwidth. Bottom: Decay profiles of **5%IrD** and **5%IrD-5%JM**, recorded at $\lambda_{em}=463$ nm, using a 375 nm laser source (inset: decay in the 0–500 ns range).

Figure 3. Top: Emission spectra of **1%IrD**, **1%JM** and **1%IrD-1%JM**, recorded from 0.3 mg mL^{-1} cyclohexane suspensions, at $\lambda_{exc}=300$ nm and 3 nm bandwidth. Bottom: Decay profiles of **1%IrD** and **1%IrD-1%JM**, recorded at $\lambda_{em}=463$ nm, using a 375 nm laser source (inset: decay in the 0–500 ns range).

the range of lifetimes to the result of different local environments experienced by the individual dye molecules, environments that determine different motional freedoms, intermolecular distances and rates of deactivation processes. Satisfactory fittings, with chi-squared values of about 1, of the recorded decay profiles were obtained by using tri-exponential functions, thus yielding three lifetime values. However, it is important to bear in mind for our consideration that the so fitted decay traces should be interpreted as the result of a generally random spatial dispersion of molecules inside the micellar template, generating a statistical distribution of intermolecular distances and decay rates, rather than simply distinct decays from exclusively three donor species.

Within this picture, for both **1%IrD** and **5%IrD** samples, the longest lifetime component is expected to correspond to isolated **IrD** molecules, protected from potential oxygen-induced quenching by residing within the core part of the mesopore channels. The fact that such long components are nearly twice as large as that of **IrD** in micromolar, deaerated solution and tending towards typical values recorded at 77 K for such compounds (3.5 μs)[59] is attributed to the strong restriction of vibrational and rotational degrees of freedom imposed by the confinement in the rigid silica environments, which also reflect into lower non-radiative rates (k_{NR} in Table 1). On the other hand, the two shorter lifetime components in both samples can be interpreted as arising from **IrD** molecules that are

within a certain proximity to one another so as to be more vulnerable to triplet-triplet annihilation and also from molecules located at the ends of the pores that may be exposed to quenching by oxygen dissolved in the cyclohexane.[66,68] Indeed, the average lifetime is reduced from 1% loading to 5% and the values of the quantum yields are lower than that of the deaerated solvated dye ($\Phi_{PL} = 0.46$), decreasing with increasing dye loading, concomitant with the enhancement of k_{NR}.

Table 2. FRET parameters for the two donor–acceptor HGCs.

Sample	τ_D [ns]	τ_{DA} [ns]	η_{ET}[a]	k_{ET} [10^5 s^{-1}][b]	r_{DA} [nm][c]
1%IrD-1%JM	2705	2047	0.24	1.19	5.7
5%IrD-5%-JM	2356	568	0.76	13.4	3.9

[a] Calculated from Equation (1) ($+/-10^{-4}$). [b] Calculated from Equation (2) ($+/-10^2$ s^{-1}). [c] Calculated from Equation (4) (error $<35\%$ assuming $k^2 = 2/3$).[71]

Two-dyes FRET antennae

The spectroscopic properties of the two-dyes HGCs were then investigated in comparison with the donor-only and the acceptor-only systems and the corresponding emission spectra and excited state lifetimes are overlaid in Figures 3 and 4.

All spectra were recorded by selective excitation at 300 nm, as this wavelength represents a local minimum in the absorbance spectrum of **JM**, but is still substantially absorbed by **IrD** with a molar extinction coefficient of about $\varepsilon = 35\,000$ M^{-1}cm^{-1}. However, due to the extensive absorbance range of BODIPY dyes, even at this local minimum, $\varepsilon = 9300$ M^{-1}cm^{-1} for **JM**. The compared spectra show evidence of quenching of **IrD** emission and sensitisation of the **JM** dye. To gain a greater understanding on the energy transfer mechanism between the two-dye species, time-resolved measurements were performed and the recorded excited state lifetimes on the two donor–acceptor systems are summarised in Table 1. As for the donor-only HGCs, tri-exponential fittings gave the most satisfactory results and a similar trend was observed for the donor–acceptor systems, in which the longest lifetime components were attributed to isolated **IrD** molecules at the core of the mesopores and the two shorter components to molecules in close proximity. Differently from the donor-only systems, though, all lifetime values were lower, as a consequence of the quenching induced by FRET, except for the shortest components, which do not undergo significant changes. Such values were therefore considered to be arising from FRET-inactive **IrD** molecules, for the reason that the efficient non-radiative deactivation pathways they are subject to very effectively outcompete FRET occurring from a triplet excited state. Such lifetime components were then excluded from the following analysis of the energy transfer parameters.

FRET analysis

The longest decay components of each system were considered to represent the simplest and most characteristic donor–acceptor pair values in the silica framework, as they are the least affected by other non-radiative deactivation routes than energy transfer. From such components, the efficiency and rate of FRET were calculated, together with estimations of average donor–acceptor distances. In doing so, we assumed a simple dipole-dipole resonance mechanism of transfer as described by Forster[69] and treated our systems, whereby donors are triplet emitters, in the same theoretical framework as that

for singlet–singlet transfer.[66,70] The values obtained from our analysis are summarised in Table 2.

The FRET efficiency was derived from:

$$E = 1 - \frac{\tau_{DA}}{\tau_D} \tag{1}$$

and resulted about three times higher for the 5:5 system than for the 1:1, with a value of 76% versus 24%. Then, to estimate the donor–acceptor distance in the two systems, the energy transfer rate k_{FRET} and the Forster distance R_0, the donor–acceptor distance, at which the FRET is 50% efficient, should be calculated. The k_{FRET} value is expressed by:

$$k_{FRET} = \frac{1}{\tau_{DA}} - \frac{1}{\tau_D} \tag{2}$$

and equals 1.19×10^5 s^{-1} for the 1:1 system, whereas it is ten times larger than for the 5:5 one.

The Forster distance R_0 is obtained from:

$$R_0 = \sqrt[6]{\left(\frac{9000 \ln 10 k^2 \phi_D J_{DA}}{128 \pi^5 N_A n^4} \right)} \tag{3}$$

in which the orientation factor $k^2 = 2/3$ (assuming an isotropic arrangement of chromophores), Φ_D was taken to be the quantum yield of deaerated **IrD** in dilute solution, 0.46, J_{DA} was previously calculated to be 2.356×10^{15} nm^{4}M^{-1}cm^{-1}, N_A is the Avogadro constant, and n was taken in this case to be the refractive index of silica, 1.552, the medium through which FRET is occurring in our systems. As a result, $R_0 = 4.9$ nm.

Finally, by using the k_{FRET} and the R_0 value in:

$$k_{FRET} = \frac{1}{\tau_{DA}} \left(\frac{R_0}{r_{DA}} \right)^6 \tag{4}$$

we obtain r_{DA} of 5.7 nm and 3.9 nm for the 1:1 and the 5:5 systems, respectively.

The calculated FRET data for the two antennae, despite the approximations and assumptions, appears to be in generally good accord with the graphical emission data. The higher rate of FRET for the 5%–5% system in comparison with that of the 1%–1% system shows that there is a positive effect from a higher loading of both donor and acceptor dyes, although the dye molecules tend to undergo increased self-quenching with

increased content. Indeed, an increase in the concentration of both the donor and acceptor species naturally leads to a strongly decreased average donor–acceptor distance, one of the key theoretical parameters involved in determining the rate of FRET. Hence, any decrease in r_{DA} will lead to a substantially amplified increase in k_{FRET}, allowing FRET processes in our antennae to even outcompete the enhanced non-radiative deactivation processes and achieve very high FRET efficiencies.

TEM imaging and mesopore dimensions

To investigate the morphology of the synthesised photoactive HGCs and to confirm that a regular mesoporous framework still defined the silica's form, TEM was performed upon the samples. Selected micrographs are presented in Figure 5. The results show that there are mesopores present in all the silica samples, which accommodate the dopant dyes, with clearly visible parallel and ordered channels, confirming that a significant degree of order is maintained up to 10% overall dye loading into the micellar template.

The FRET donor–acceptor distances for the HGCs (Table 2) are on the same order of magnitude as the pore widths as expected. The fact that the pore diameters are roughly the same as the donor–acceptor distances of the 1%:1% system may imply that the dyes are not placed at the same intervals through the cylindrical mesophases but alternate, so that the distance between them is greater than the cross-sectional radius. With increased dye loading to 5%:5%, the average r_{DA} value becomes closer to the micellar radius, however, further studies and more accurate pore size data are necessary to elu-

cidate the connection between these distances and the precise localisation of donor and acceptor species.

Conclusions

A new design of artificial FRET antenna for light-harvesting has been presented, utilising the template-assisted host-guest chemistry of the mesoporous organosilica, COK-12, to encapsulate a near-UV-absorbing, blue-emitting donor iridium tris-chelate complex (**IrD**) and a blue-absorbing, green-yellow-emitting BODIPY dye (**JM**), which were designed to reside, respectively, within the lipophilic centre of the templating micellar mesophase and along the surfactant chains inside the template.

When a 1% loading of **IrD** only is included into the COK-12 silica, the photophysical properties are found to generally change in a manner consistent with the effective shielding and protection of the dye from oxygen and the retardation of non-radiative deactivation processes, demonstrated by an increase in the longest recorded excited state lifetime compared to solvated **IrD**.

With the inclusion of **JM** also, acting as the acceptor dye, **IrD** proved to be a capable donor dye for the COK-12-encapsulated FRET antennae, yielding average FRET efficiencies amongst FRET-active molecules as high as 76% for the 5%:5% loaded system. Despite the growth of non-radiative deactivation rates, a limited increase in both donor and acceptor loadings, maintaining a 1:1 molar ratio, results in an increase in both rate and efficiency of FRET, with retention of the mesoporous order of the silica framework.

COK-12 mesoporous silica has therefore proven to be a robust and effective host for the encapsulation of multiple dye species and for enabling a degree of control over the donor–acceptor distance in artificial FRET antennae in the production of host-guest compounds with inbuilt optical functionalities, and, furthermore, **IrD** and its derivatives have been shown to have considerable potential as photosensitisers for BODIPY-based light-harvesting systems.

Experimental Section

Materials and Methods

All air- and water-sensitive experiments were performed under a nitrogen atmosphere by using standard vacuum-line techniques. All chemicals were obtained commercially and used without further purification. "H_2O" refers to high purity water with conductivity of 0.04 $\mu S\,cm^{-1}$, obtained from a Milli-Q purification system. Thin-layer chromatography (TLC) was carried out on silica plates (silica gel 60 F254, Merck 5554) and visualized by UV lamp (254 nm). Preparative column chromatography was carried out using silica gel (Merck Silica Gel 60, 230±400 mesh) pre-soaked in the starting eluent. ^1H and ^{13}C NMR spectra were recorded with either Agilent MR400DD2 400 MHz, Bruker AVANCE 300 MHz or JEOL 400 MHz spectrometers operating at 25°C. Transmission electron microscopy images were taken on a 100 kV CM100 TEM (FEI).
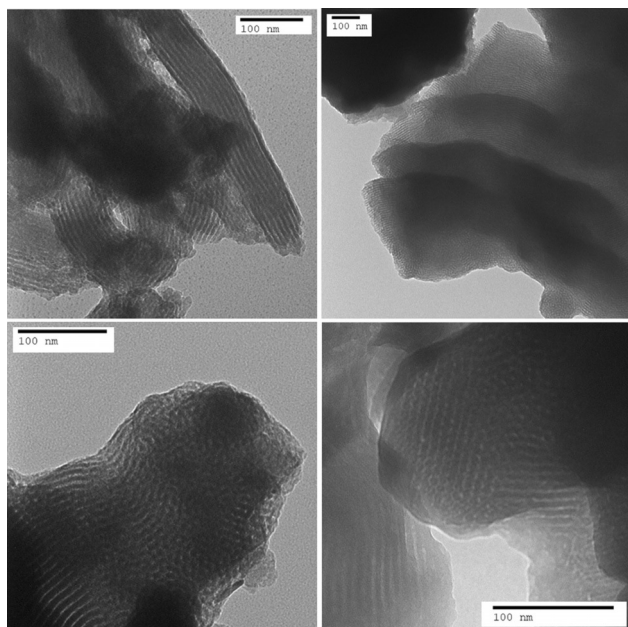
Figure 5. TEM images of the silica samples doped HGCs: 1%IrD (top left), 1%IrD-1%JM (top right), 5%IrD (bottom left) and 5%IrD-5%JM (bottom right). The estimated range of pore diameters by cursory inspection of these images spans 5–10 nm, in agreement with the literature.[49]

Synthesis of COK-12 silica with 100% P123 micelles

Pluronic-P123 (1.02 g, 0.174 mmol), citric acid monohydrate (953 mg, 4.96 mmol), and trisodium citrate dihydrate (803 mg, 3.11 mmol) were stirred in H_2O (27 mL) for 1.5 h, during which the solution turned clear. Sodium silicate/H_2O solution (1.8 mL, 21.97 mmol) was diluted with H_2O (7.5 mL) and added dropwise to the reaction mixture. The mixture was stirred for 10 min, turning cloudy. It was left undisturbed for 24 h, during which a white precipitate formed, then the mixture was filtered under vacuum. The solid residue was washed with H_2O, producing foam. Washing was repeated until the foaming ceased. The solid was then dried in an oven overnight, leading to a white powdery solid.

Synthesis of COK-12 silica with mixed P123 and JM micelles

Citric acid monohydrate (954 mg, 4.97 mmol) and trisodium citrate dihydrate (793.5 mg, 3.07 mmol), were dissolved in H_2O. To this solution, Pluronic-P123 and both JM and IrD dyes were added in the following ratios, to achieve the intended dye loadings: 98:1:1 (0.169 mmol P123, 1.71 μmol JM, 1.71 μmol IrD) and 90:5:5 (0.162 mmol P123, 8.54 μmol JM, 8.54 μmol IrD). The IrD was added from a 5.73×10^{-4} M acetonitrile stock solution after P123 and JM were dissolved upon sonication. The solution was stirred in H_2O (27 mL) overnight, during which it turned iridescent red-yellow. Sodium silicate/H_2O solution (1.75 mL, 21.36 mmol) was then added dropwise to the reaction mixture, which was stirred for 10 minutes, turning a cloudy pink. This was then left undisturbed for 24 hours, during which a pink precipitate formed. The mixture was filtered under vacuum, and the retentate was washed with H_2O, producing foam. Washing was repeated until the foaming ceased. The retentate was then dried in a vacuum desiccator at RT overnight, producing powdery solids which photoluminesced bright green under UV light.

UV/Vis spectroscopy

Absorption spectra were recorded using a Shimadzu UV-1800 spectrophotometer. Fluorescence spectra and lifetimes were measured using an Edinburgh FLS980 photoluminescence spectrometer, equipped with a 450 W Xenon arc lamp, Czerny Turner excitation and emission monochromators (1.8 nm mm^{-1} dispersion; 1800 grooves mm^{-1}), time-correlated single photon counting (TCSPC) module and a Hamamatsu R928P photomultiplier tube (in fan assisted TE cooled housing, operating temperature $-20\,°C$). For lifetime measurements, samples were excited with an EPL-375 (370.8 nm; 61.1 ps pulse width) and an EPL-475 (471.8 nm; 61.1 ps pulse width) picosecond pulsed diode lasers and data analysis was performed on the F980 software with numerical data reconvolution based on Marquardt-Levenberg algorithm. Luminescence quantum yields were measured using as reference an aqueous solution of quinine sulfate (0.5 M NaOH; $\varphi = 0.87$).

Conflict of interest

The authors declare no conflict of interest.

[1] V. Balzani, M. Venturi, A. Credi, *Molecular Devices and Machines-A Journey Into the Nanoworld, Vol. 17*, Wiley-VCH, Weinheim, **2003**.

[2] S. Liu, Z.-R. Tang, Y. Sun, J. C. Colmenares, Y.-J. Xu, *Chem. Soc. Rev.* **2015**, *44*, 5053 – 5075.

[3] L. Jullien, J. Canceill, B. Valeur, E. Bardez, J.-M. Lehn, *Angew. Chem. Int. Ed. Engl.* **1994**, *33*, 2438 – 2439; *Angew. Chem.* **1994**, *106*, 2582 – 2584.

[4] V. Balzani, S. Campagna, G. Denti, A. Juris, S. Serroni, M. Venturi, *Acc. Chem. Res.* **1998**, *31*, 26 – 34.

[5] D. Gust, T. A. Moore, A. L. Moore, *Pure Appl. Chem.* **1998**, *70*, 2189 – 2200.

[6] W. S. Aldridge III, B. J. Hornstein, S. Serron, D. M. Dattelbaum, J. R. Schoonover, T. J. Meyer, *J. Org. Chem.* **2006**, *71*, 5186 – 5190.

[7] C. N. Fleming, P. Jang, T. J. Meyer, J. M. Papanikolas, *J. Phys. Chem. B* **2004**, *108*, 2205 – 2209.

[8] G. Calzaferri, H. Maas, M. Pauchard, M. Pfenniger, S. Megelski, A. Devaux in *Advances in Photochemistry, Vol. 27* (Eds.: D. C. Neckers, G. Von Bunau, W. S. Jenks), Wiley, Hoboken, **2002**, Chap. 1.

[9] N. Armaroli, V. Balzani, *Angew. Chem. Int. Ed.* **2007**, *46*, 52 – 66; *Angew. Chem.* **2007**, *119*, 52 – 67.

[10] V. Balzani, A. Credi, M. Venturi, *ChemSusChem* **2008**, *1*, 26 – 58.

[11] A. Devaux, F. Cucinotta, S. Kehr, L. De Cola in *Functional Supramolecular Architectures for Organic Electronics and Nanotechnology, Vol. 1* (Eds.: P. Samorí, F. Cacialli), Wiley-VCH, Weinheim, **2010**, p. 283.

[12] Y. H. Jeong, M. Son, H. Yoon, P. Kim, D. H. Lee, D. Kim, W. D. Jang, *Angew. Chem. Int. Ed.* **2014**, *53*, 6925 – 6928; *Angew. Chem.* **2014**, *126*, 7045 – 7048.

[13] W. Q. Wu, H. L. Feng, H. S. Rao, Y. F. Xu, D. B. Kuang, C. Y. Su, *Nat. Commun.* **2014**, *5*, 1 – 9.

[14] A. Adronov, S. L. Gilat, J. M. J. Frechet, K. Ohta, F. V. R. Neuwahl, G. R. Fleming, *J. Am. Chem. Soc.* **2000**, *122*, 1175 – 1185.

[15] E. K. L. Yeow, K. P. Ghiggino, J. N. H. Reek, M. J. Crossley, A. W. Bosman, A. P. H. J. Schenning, E. W. Meijer, *J. Phys. Chem. B* **2000**, *104*, 2596 – 2606.

[16] E. La Mazza, F. Puntoriero, F. Nastasi, B. Larámee-Milette, G. S. Hanan, S. Campagna, *Dalton Trans.* **2016**, *45*, 19238 – 19241.

[17] L. Jullien, J. Canceill, B. Valeur, E. Bardez, J.-M. Lehn, *Angew. Chem. Int. Ed. Engl.* **1994**, *33*, 2438 – 2439; *Angew. Chem.* **1994**, *106*, 2582 – 2584.

[18] T. Ikeda, Y. Ueda, N. Komori, M. Abe, T. Haino, *Supramol. Chem.* **2017**, *29*, 471 – 476.

[19] K. V. Rao, K. K. R. Datta, M. Eswaramoorthy, S. J. George, *Angew. Chem. Int. Ed.* **2011**, *50*, 1179 – 1184; *Angew. Chem.* **2011**, *123*, 1211 – 1216.

[20] A. Ajayaghosh, V. K. Praveen, C. Vijayakumar, *Chem. Soc. Rev.* **2008**, *37*, 109 – 122.

[21] N. Aratani, D. Kim, A. Osuka, *Acc. Chem. Res.* **2009**, *42*, 1922 – 1934.

[22] J. Yang, M. C. Yoon, H. Yoo, P. Kim, D. Kim, *Chem. Soc. Rev.* **2012**, *41*, 4808 – 4826.

[23] P. K. Dutta, R. Varghese, J. Nangreave, S. Lin, H. Yan, Y. Liu, *J. Am. Chem. Soc.* **2011**, *133*, 11985 – 11993.

[24] C. M. Spillmann, I. L. Medintz, *J. Photochem. Photobiol. C* **2015**, *23*, 1 – 24.

[25] Q. L. Zou, K. Liu, M. Abbas, X. H. Yan, *Adv. Mater.* **2016**, *28*, 1031 – 1043.

[26] P. Ensslen, H. A. Wagenknecht, *Acc. Chem. Res.* **2015**, *48*, 2724 – 2733.

[27] G. D. Scholes, G. Rumbles, *Nat. Mater.* **2006**, *5*, 683 – 696.

[28] K. W. J. Barnham, J. L. Marques, J. Hassard, P. O'Brien, *Appl. Phys. Lett.* **2000**, *76*, 1197 – 1201.

[29] a) D. H. Holden, J. E. Guillet, *Macromolecules* **1980**, *13*, 289 – 295; b) B. Jana, S. Bhattacharyya, A. Patra, *Nanoscale* **2016**, *8*, 16034 – 16043.

[30] A. Hennig, S. Hatami, M. Spieles, U. Resch-Genger, *Photochem. Photobiol. Sci.* **2013**, *12*, 729 – 737.

[31] A. T. Hädler, K. Kreger, A. Issac, B. Wittmann, M. Kivala, N. Hammer, J. Köhler, H. W. Schmidt, R. Hildner, *Nature* **2015**, *523*, 196 – 200.

[32] C. D. Bösch, S. M. Langenegger, R. Häner, *Angew. Chem. Int. Ed.* **2016**, *55*, 9961 – 9964; *Angew. Chem.* **2016**, *128*, 10115 – 10118.

[33] E. Collini, G. D. Scholes, *Science* **2009**, *323*, 369 – 373.

[34] F. Hoffmann, M. Fröba, *Chem. Soc. Rev.* **2011**, *40*, 608 – 620.

[35] J. Gierschner, *Phys. Chem. Chem. Phys.* **2012**, *14*, 13146 – 13153.

[36] P. Cao, O. Khorev, A. Devaux, L. Sägesser, A. Kunzmann, A. Ecker, R. Häner, D. Brühwiler, G. Calzaferri, P. Belser, *Chem. Eur. J.* **2016**, *22*, 4046 – 4060.

[37] F. Cucinotta, F. Carniato, A. Devaux, L. De Cola, L. Marchese, *Chem. Eur. J.* **2012**, *18*, 15310 – 15315.

[38] B. M. Estevão, F. Cucinotta, N. Hioka, M. Cossi, M. Argeri, G. Paul, L. Marchese, E. Gianotti, *Phys. Chem. Chem. Phys.* **2015**, *17*, 26804 – 26812.

[39] G. Calzaferri, R. Méallet-Renault, D. Brühwiler, R. Pansu, I. Dolamic, T. Dienel, P. Adler, H. Li, A. Kunzmann, *ChemPhysChem* **2011**, *12*, 580 – 594.

[40] G. Tabacchi, *ChemPhysChem* **2018**, *19*, 1249 – 1297.

[41] D. Tleugabulova, Z. Zhang, J. D. Brennan, *J. Phys. Chem. B* **2002**, *106*, 13133 – 13138.

[42] G. Calzaferri, S. Huber, H. Maas, C. Minkowski, *Angew. Chem. Int. Ed.* **2003**, *42*, 3732 – 3758; *Angew. Chem.* **2003**, *115*, 3860 – 3888.

[43] N. Mizoshita, T. Taniab, S. Inagaki, *Chem. Soc. Rev.* **2011**, *40*, 789 – 800.

[44] A. Devaux, G. Calzaferri, P. Belser, P. P. Cao, D. Bruhwiler, A. Kunzmann, *Chem. Mater.* **2014**, *26*, 6878 – 6885.

[45] a) C. Kresge, M. Leonowicz, W. Roth, J. Vartuli, J. Beck, *Nature* **1992**, *359*, 710 – 712; b) J. E. Lofgreen, G. A. Ozin, *Chem. Soc. Rev.* **2014**, *43*, 911 – 933.

[46] a) L. Grösch, Y. J. Lee, F. Hoffmann, M. Fröba, *Chem. Eur. J.* **2015**, *21*, 331 – 346; b) S. Inagaki, S. Guan, T. Ohsuna, O. Terasaki, *Nature* **2002**, *416*, 304 – 307; c) X. Liu, Y. Maegawa, Y. Goto, K. Hara, S. Inagaki, *Angew. Chem. Int. Ed.* **2016**, *55*, 7943 – 7947; *Angew. Chem.* **2016**, *128*, 8075 – 8079.

[47] F. Cucinotta, B. P. Jarman, C. Caplan, S. J. Cooper, H. J. Riggs, J. Martinelli, K. Djanashvili, E. L. Mazza, F. Puntoriero, *ChemPhotoChem* **2018**, *2*, 196 – 206.

[48] a) M. D. B. E. S. Botelho, J. M. Fernandez-Hernandez, T. B. de Queiroz, H. Eckert, L. De Cola, A. S. S. de Camargo, *J. Mater. Chem.* **2011**, *21*, 8829 – 8834; b) T. B. de Queiroz, M. B. S. Botelho, J. M. Fernandez-Hernandez, H. Eckert, R. Q. Albuquerque, A. S. S. de Camargo, *J. Phys. Chem. C* **2013**, *117*, 2966 – 2975.

[49] a) J. Jammaer, A. Aerts, J. D'Haen, J. W. Seo, J. A. Martens, *J. Mater. Chem.* **2009**, *19*, 8290 – 8293; b) G. Wanka, H. Hoffmann, W. Ulbricht, *Macromolecules* **1994**, *27*, 4145 – 4159.

[50] A. Loudet, K. Burgess, *Chem. Rev.* **2007**, *107*, 4891 – 4932.

[51] G. Ulrich, R. Ziessel, A. Harriman, *Angew. Chem. Int. Ed.* **2008**, *47*, 1184 – 1201; *Angew. Chem.* **2008**, *120*, 1202 – 1219.

[52] S. Choi, J. Bouffard, Y. Kim, *Chem. Sci.* **2014**, *5*, 751 – 755.

[53] D. Tleugabulova, Z. Zhang, J. D. Brennan, *J. Phys. Chem. B* **2002**, *106*, 13133 – 13138.

[54] a) H. Maas, G. Calzaferri, *Angew. Chem. Int. Ed.* **2002**, *41*, 2284 – 2287; *Angew. Chem.* **2002**, *114*, 2389 – 2392; b) O. Bossart, L. De Cola, S. Welter, G. Calzaferri, *Chem. Eur. J.* **2004**, *10*, 5771 – 5775.

[55] T. T. Vu, M. Dvorko, E. Y. Schmidt, J.-F. Audibert, P. Retailleau, B. A. Trofimov, R. B. Pansu, G. Clavier, R. Méallet-Renault, *J. Phys. Chem. C* **2013**, *117*, 5373 – 5385.

[56] P. D. Frischmann, K. Mahata, F. Würthner, *Chem. Soc. Rev.* **2013**, *42*, 1847 – 1870.

[57] L. Flamigni, A. Barbieri, C. Sabatini, B. Ventura, F. Barigelletti, *Top. Curr. Chem.* **2007**, *281*, 143 – 203.

[58] Y. You, W. Nam, *Chem. Soc. Rev.* **2012**, *41*, 7061 – 7084.

[59] a) C. A. Strassert, M. Mauro, L. De Cola, *Adv. Inorg. Chem.* **2011**, *63*, 47 – 103; b) E. Orselli, G. S. Kottas, A. E. Konradsson, P. Coppo, R. Fröhlich, L. De Cola, A. V. Dijken, M. Büchel, H. Börner, *Inorg. Chem.* **2007**, *46*, 11082 – 11093.

[60] A. Beeby, S. Bettington, I. D. W. Samuel, Z. J. Wang, *J. Mater. Chem.* **2003**, *13*, 80 – 83.

[61] H. Yersin, *Highly Efficient OLEDs with Phosphorescent Materials*, Wiley-VCH, Weinheim, **2008**.

[62] M. A. Baldo, S. Lamansky, P. E. Burrows, M. E. Thompson, S. R. Forrest, *Appl. Phys. Lett.* **1999**, *75*, 4 – 6.

[63] S. Lamansky, P. Djurovich, D. Murphy, F. Abdel-Razzaq, R. Kwong, I. Tsyba, M. Bortz, B. Mui, R. Bau, M. E. Thompson, *Inorg. Chem.* **2001**, *40*, 1704 – 1711.

[64] J. H. Burroughes, D. D. C. Bradley, A. R. Brown, R. N. Marks, K. Mackay, R. H. Friend, P. L. Burns, A. B. Holmes, *Nature* **1990**, *347*, 539 – 541.

[65] R. D. Costa, E. Orti, H. J. Bolink, F. Monti, G. Accorsi, N. Armaroli, *Angew. Chem. Int. Ed.* **2012**, *51*, 8178 – 8211; *Angew. Chem.* **2012**, *124*, 8300 – 8334.

[66] F. Cucinotta, A. Guenet, C. Bizzarri, W. Mróz, C. Botta, B. Milián-Medina, J. Gierschner, L. De Cola, *ChemPlusChem* **2014**, *79*, 45 – 57.

[67] S. Preus, a | e-UV/Vis-IR Spectral Software 2.2, FluorTools, https://www.fluortools.com.

[68] J. D. Wild, T. Sridhar, O. E. Potter, *Chem. Eng. J.* **1978**, *15*, 209 – 214.

[69] a) T. Förster, *Ann. Phys.* **1948**, *437*, 55 – 75; b) T. Förster, *Discuss. Faraday Soc.* **1959**, *27*, 7 – 17.

[70] R. G. Bennett, R. P. Schwenker, R. E. Kellogg, *J. Chem. Phys.* **1964**, *41*, 3040 – 3041.

[71] J. R. Lakowicz, *Principles of Fluorescence Spectroscopy, 3rd ed.*, Springer, New York, **2006**.